

Electrooptic Modulation of Silicon-on-Insulator Submicrometer-Size Waveguide Devices

C. Angulo Barrios, V. R. Almeida, *Student Member, IEEE, Student Member, OSA*, R. Panepucci, and M. Lipson, *Member, IEEE, Member, OSA*

Abstract—In this paper, we propose and analyze an electrically modulated silicon-on-insulator (SOI) submicrometer-size high-index-contrast waveguide. The geometry of the waveguide provides high lateral optical confinement and defines a lateral p-i-n diode. The electrooptic structure is electrically and optically modeled. The effect of the waveguide geometry on the device performance is studied. Our calculations indicate that this scheme can be used to implement submicrometer high-index-contrast waveguide active devices on SOI. As an example of application, a one-dimensional microcavity intensity modulator is predicted to exhibit a modulation depth as high as 80% by employing a dc power consumption as low as $14 \mu\text{W}$.

Index Terms—Device modeling, integrated optics, plasma dispersion effect, silicon optoelectronics.

I. INTRODUCTION

SILICON as a photonic medium has unique advantages. It is transparent in the range of optical telecommunication wavelengths (1.3 and $1.55 \mu\text{m}$) and has a high index of refraction, which allows for the fabrication of high-index-contrast submicrometer structures [1]. In addition, the mature Si integrated circuit [bipolar or complementary metal-oxide semiconductor (CMOS)] technology enables the implementation of dense silicon-based integrated optics and electronics on-chip. In order to achieve low-loss compact (submicrometer size) devices, high refractive index contrast is required. For this purpose, silicon-on-insulator (SOI) strip waveguide technology may be employed [1] [see Fig. 1(a)]. The use of crystalline Si (c-Si) instead of polysilicon or amorphous Si as the waveguide core reduces scattering and absorption losses [2].

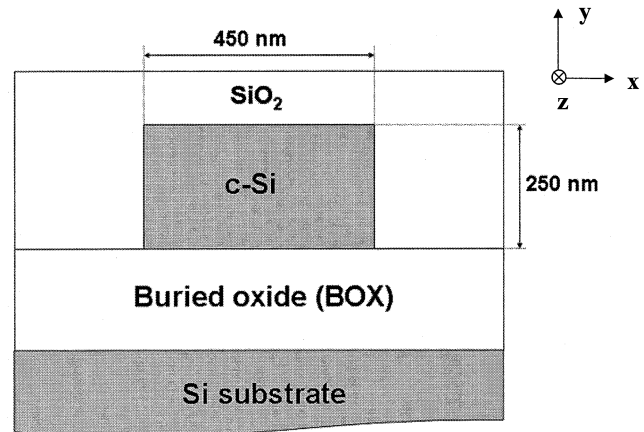
Passive submicrometer-size structures such as ultra-low-loss strip waveguides [3], efficient couplers [4], microring resonators [5], and nanocavities [6] on SOI have been demonstrated. Active waveguide devices (modulators and switches), however, have been proposed only on large micrometer-size SOI waveguides [7], [8]. Very little work has been reported on high-index-contrast (high lateral optical confinement) waveguide active devices despite their high demand to manipulate light beams for information processing (e.g., coding-decoding, routing, multiplexing, timing, logic operations, etc.) in high-density integrated-optic circuits.

The main methods to alter the refractive index in Si are the thermo-optic effect and the electrooptic effect. The thermal change of the real optical refractive index in Si is large [9].

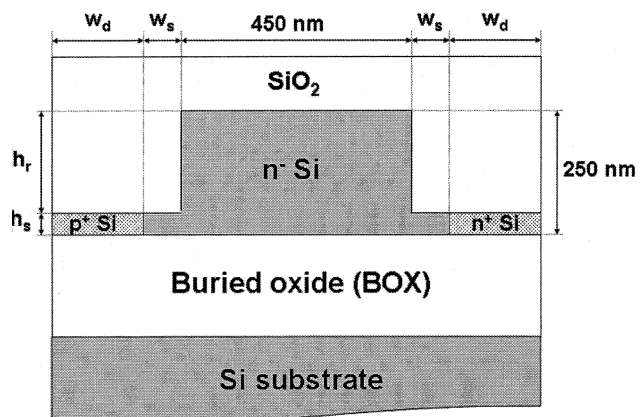
Manuscript received April 1, 2003; revised July 9, 2003.

The authors are with the School of Electrical and Computer Engineering, Cornell University, Ithaca, NY 14853 USA.

Digital Object Identifier 10.1109/JLT.2003.818167



(a)



(b)

Fig. 1. Schematic cross-section of (a) a typical SOI high-index-contrast strip waveguide for $1.55 \mu\text{m}$ wavelength and (b) the counterpart rib waveguide with an integrated lateral p-i-n diode for electrooptic modulation.

However, the thermo-optic effect is rather slow and can be used only up to 1-MHz modulation frequencies [10]. For higher modulation frequencies, up to a few hundreds of megahertz, electrooptic devices are required. Unstrained pure crystalline Si does not exhibit linear electrooptic (Pockels) effect, and the refractive index changes due to the Franz-Keldysh effect and Kerr effect are very weak. Therefore, the free carrier dispersion effect [11] is used to change both the real refractive index and optical absorption coefficient.

The free-carrier concentration in electrooptic devices can be varied by injection, accumulation, depletion, or inversion of carriers. P-i-n diodes and metal-oxide-semiconductor field-effect transistors (MOSFET) may be employed for this purpose. The use of a MOS diode should lead to high-speed operation and no

dc power consumption. However, for either depletion or accumulation, significant large concentration variations are possible only within small distances (a few tens of nanometers) beneath the insulated gate region. This produces a small overlap between the optical mode and the nonequilibrium charge (index change) distribution in the waveguide, leading to a small effective index variation. In contrast, in a p-i-n configuration, carriers can be injected in a larger area (intrinsic region) in order to maximize the aforementioned overlap, increasing the effective index change. In this case, the p-i-n diode should be designed in such a way that the highly doped p- and n-regions should neither significantly affect the optical mode confinement nor introduce excessive losses. In addition, the electrical power needed for changing the index should be low in order to minimize the thermo-optic effect.

In this paper, we analyze an electrooptic configuration for varying the complex refractive index of high-index-contrast SOI waveguides by using a lateral p-i-n diode. Section II describes the waveguide structure. Section III presents the electrical and optical models. In Section IV, the results from the simulations are presented and discussed. In Section V, an intensity modulator based on a one-dimensional microcavity is analyzed as an example of application. Conclusions are given in Section V.

II. STRUCTURE

Fig. 1(b) shows a schematic cross-section of the proposed configuration. It consists of a high-aspect-ratio [rib height (h_r) \gg slab height (h_s)] rib SOI waveguide with a p⁺ region and an n⁺ region defined in the slab at each side of the rib. The silicon layer (device layer) has an n-type background doping concentration of 10^{15} cm⁻³, whereas a uniform doping concentration of 10^{19} cm⁻³ for both p⁺ and n⁺ regions is considered. We have assumed typical values for the height and width of a 1.55- μ m-wavelength high-index-contrast strip SOI waveguide, 250 and 450 nm, respectively [4]. The width of the doped regions and their distance to the rib sidewalls are referred to as w_d and w_s , respectively. A top SiO₂ cladding layer covers the whole structure.

III. DEVICE MODEL

A. Optical Model

We used the beam propagation method (BPM)¹ for the calculation of the modal-field profile and optical losses due to carrier absorption. From the values of the electron and hole concentrations at any point of the p-i-n structure (calculated with the electrical model described below), the induced real refractive index and optical absorption coefficient variations (Δn and $\Delta\alpha$, respectively) produced by free-carrier dispersion (highly doped regions and injected carriers) at a wavelength of 1.55 μ m are calculated by using [12]

$$\begin{aligned} \Delta n &= \Delta n_e + \Delta n_h \\ &= - [8.8 \times 10^{-22} \cdot \Delta N + 8.5 \times 10^{-18} \cdot (\Delta P)^{0.8}] \quad (1) \end{aligned}$$

$$\begin{aligned} \Delta\alpha &= \Delta\alpha_e + \Delta\alpha_h \\ &= 8.5 \times 10^{-18} \cdot \Delta N + 6.0 \times 10^{-18} \Delta P \quad (2) \end{aligned}$$

¹<http://www.rssoftinc.com/fullwave.htm>.

where

Δn_e	refractive index change due to electron concentration change;
Δn_h	refractive index change due to hole concentration change;
ΔN	electron concentration change in cm ⁻³ ;
ΔP	hole concentration change in cm ⁻³ ;
$\Delta\alpha_e$ (in cm ⁻¹)	absorption coefficient variations due to ΔN ;
$\Delta\alpha_h$ (in cm ⁻¹)	the absorption coefficient variation due to ΔP .

B. Electrical Model

A commercially available two-dimensional simulation package, ATLAS from SILVACO,² was employed to achieve the electrical calculations. The suitability of this device modeling software to analyze electrooptic modulators in SOI waveguides has been demonstrated by other authors [13], [14]. This program simulates internal physics and device characteristics of semiconductor devices by solving Poisson's equation and the charge continuity equations for electrons and holes numerically. The software allows a complete statistical approach (Fermi–Dirac statistics) when, for example, heavily doped regions are considered. Carrier recombination models include Shockley–Read–Hall (SRH) recombination, Auger recombination, and surface recombination. A concentration and temperature-dependent model has been used for the carrier mobility. The simulation package also includes thermal modeling, which accounts for Joule heating, and heating and cooling due to carrier generation and recombination. The heat flow equation is solved for specific combination of heat sink structures, thermal impedances, and ambient temperatures.

In our calculations, a carrier concentration dependent SRH recombination model has been employed, with an estimated carrier lifetime in the Si device layer (intrinsic region) of electrons and holes of $\tau_n = 700$ ns and $\tau_p = 300$ ns, respectively, for an n-type doping concentration of 10^{15} cm⁻³ [15].

Ohmic contacts without additional contact resistance or capacitance have been assumed. In addition, the electrical contacts (electrodes) were considered to act as thermal contacts (heat sinks) at a fixed temperature of 300 K. The main parameters used in the simulations are shown in Table I.

IV. RESULTS AND DISCUSSION

In this section, coupling efficiency from a strip waveguide to the waveguide modulator, losses due to absorption in the waveguide, and the effect of the overlap between the optical mode and the high absorption regions are analyzed. Then, the optimum optical design is studied in order to determine dc power consumption, device temperature, and transient response.

A. Optical Characteristics

1) *Modal Behavior:* Both waveguides shown in Fig. 1(a) and (b) exhibit single-mode operation for both TE-like and TM-like modes and slab thicknesses of $h_s = 30, 50, \text{ and } 70$ nm. The

²SILVACO International, Santa Clara, CA.

TABLE I
MAIN PARAMETERS USED IN THE SIMULATIONS

Si refractive index ($\lambda=1.55 \mu\text{m}$)	3.43
SiO ₂ refractive index ($\lambda=1.55 \mu\text{m}$)	1.46
Electron carrier lifetime τ_n (ns)	700 ^a
Hole carrier lifetime τ_p (ns)	300 ^a
Surface recombination velocity for electrons S_n (cm/s)	10 ^{2b}
Surface recombination velocity for holes S_p (cm/s)	10 ^{2b}
Si background carrier conc. (cm ⁻³)	1x10 ¹⁵
Thermal contacts temperature (K)	300
Si thermal conductivity κ (W/cmK) at 300 K	1.55
Si heat capacity C (J/cm ³) at 300 K	1.67

^a For an electron concentration of 10¹⁵ cm⁻³ at 300 K (From Ref. 15)

^b For a thermally oxidized Si surface (From Ref. 16)

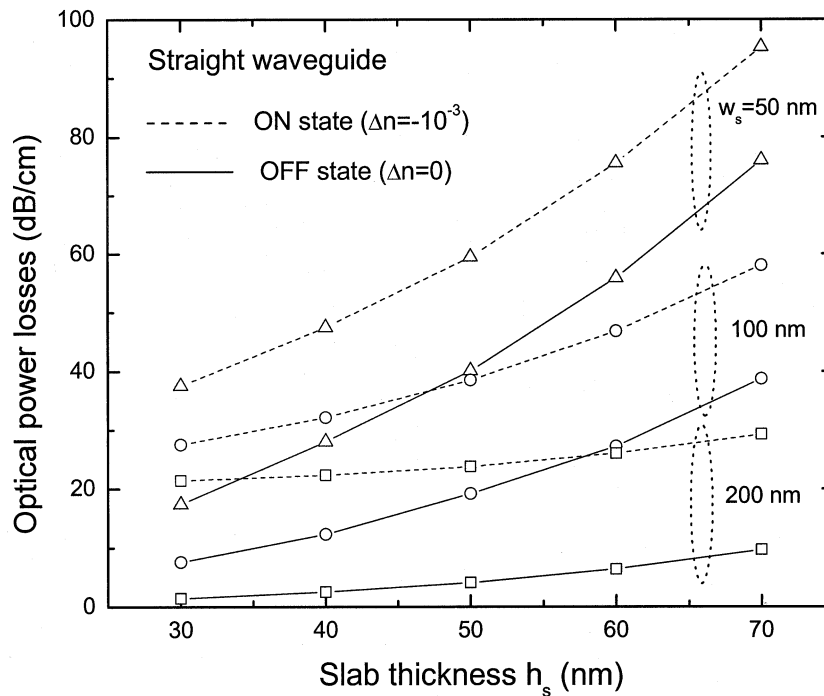


Fig. 2. Optical losses in a straight high-index-contrast rib waveguide as a function of the slab thickness (h_s) in the OFF state (solid line) and ON state (dashed line) for a distance of the highly doped regions to the rib sidewall (w_s) of 200 nm (square dots), 100 nm (circular dots), and 50 nm (triangular dots).

calculated optical mode overlap between the strip and the high-index-contrast rib waveguides was as high as 99.7%, 99.3%, and 98.6% for slab thickness of 30, 50, and 70 nm, respectively. That is, the introduction of the thin slab does not affect significantly the mode distribution in the rib waveguide as compared to the strip waveguide. This is important in order to obtain a good cou-

pling efficiency from (to) the high-index-contrast rib waveguide into (from) a fiber-to-waveguide coupler implemented in a strip waveguide [4].

2) *Loss Analysis:* The distance of the highly doped regions to the rib sidewalls (w_s) should be long enough to reduce the overlap of these highly absorptive regions with the guided op-

tical mode but short enough to minimize the power consumption and switching time. Similarly, the thickness of the slab (h_s) should be thin enough to provide a high lateral optical confinement and to reduce the overlap of the highly doped regions with the optical field but thick enough to facilitate its practical implementation. Fig. 2 shows the calculated optical losses due to carrier absorption for a high-index-contrast rib waveguide as a function of h_s for different values of w_s . Two cases are considered: 1) no carrier injection (OFF state) and 2) uniform carrier injection (ON state) of $N = P = 3 \times 10^{17} \text{ cm}^{-3}$ throughout the whole intrinsic region, which induces a real refractive index change of $\Delta n = -10^{-3}$ (1) and an absorption coefficient variation of $\Delta\alpha = 4.35 \text{ cm}^{-1}$ (2). The validity of considering $N = P$ with a uniform distribution will be supported by the electrical analysis in Section IV-B. The variation of the real part of the effective refractive index of the waveguide is approximately the same as that in the intrinsic Si core, that is, $\Delta n_{\text{eff}} = -10^{-3}$. It is seen in Fig. 2 that the losses are high for $w_s = 50 \text{ nm}$ (38–95 dB/cm in the ON state and 17–76 dB/cm in the OFF state) and all the considered values of h_s , even when no carriers are injected. This is because of the proximity of the highly doped (highly absorptive) regions to the rib, which increases the overlap with the optical mode. On the other hand, the losses are significantly lower (21–29 dB/cm in the ON state and 1.4–9.7 dB/cm in the OFF state) when the doped regions are separated from the rib sidewall $w_s = 200 \text{ nm}$. Fig. 2 also shows that the losses increase as h_s increases for a given w_s . This is due to the fact that the thicker the slab, the more the optical mode-field profile extends laterally and overlaps with the highly doped regions, increasing the losses. In all cases, a remarkable increment of the optical losses is observed when carriers are injected. This increase is higher as the thickness of the slab increases because of the larger absorption area due to injected carriers.

Another requisite that w_s and h_s should fulfill is being able to implement bent waveguides with a small radius of curvature without introducing significant losses. This is important in order to produce high dense photonic circuits. Fig. 3(a) and (b) illustrates the optical mode distributions in a bent waveguide turning to the left ($-x$ -axis) with a radius of curvature of $5 \mu\text{m}$ and a straight waveguide, respectively, in the ON state. $w_s = 50 \text{ nm}$ and $h_s = 200 \text{ nm}$ for both cases. It is observed in Fig. 3(a) that the optical field shifts to the right side ($+x$ -axis) due to the bending effect, overlapping significantly the doped region placed on that side of the bend (n^+ region). The straight waveguide counterpart in Fig. 3(b) is shown for comparison purposes. Fig. 4 presents the calculated optical losses for high-index-contrast rib straight and bent (radius = $5 \mu\text{m}$) waveguides as a function of h_s for different values of w_s in the ON state (carrier injection $N = P = 3 \times 10^{17} \text{ cm}^{-3}$). The losses due to the bend become important as the slab thickness increases for a given w_s . This is because the higher h_s is, the deeper the lateral penetration of the optical mode into the convex (outer) slab side of the bend is, increasing the overlap with the highly absorptive regions. It is also seen that the difference in loss between the straight and bent waveguides increases as w_s decreases for a given slab thickness. This occurs because the closer the doped regions are to the rib, the higher the overlap is between them and the shifted optical field.

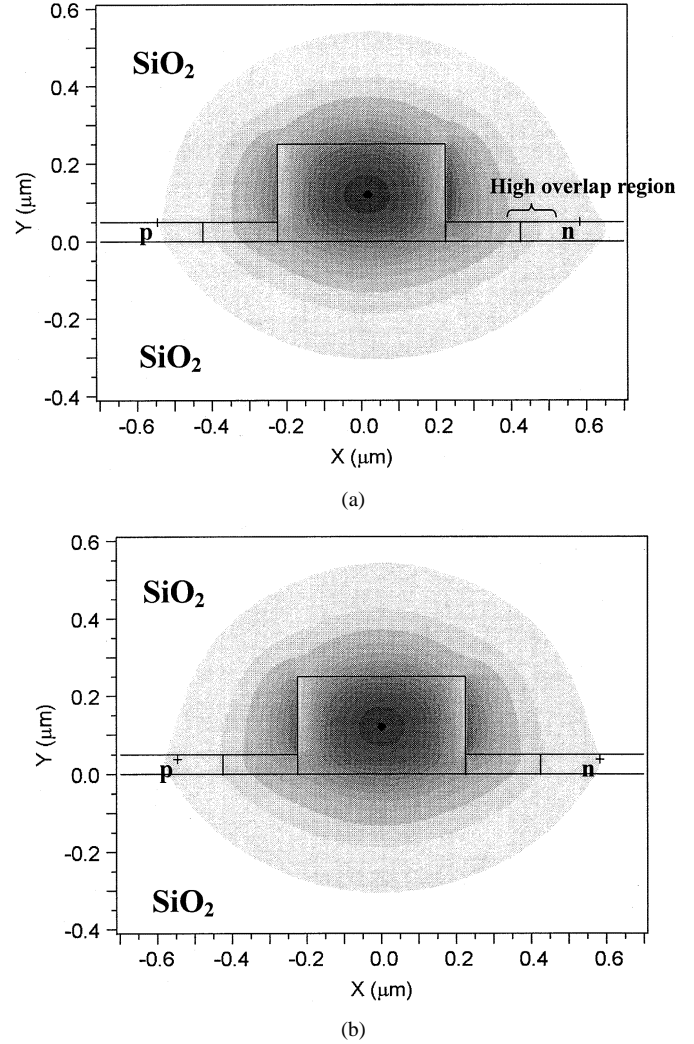


Fig. 3. TE-like fundamental optical mode-field profile in (a) a high-index-contrast rib bent waveguide, which turns to the $-x$ -axis (left) and (b) a straight high-index-contrast waveguide. The mode distribution in the bend is shifted to the convex side of the bend ($+x$ -axis).

These results show that, from the optical point of view, a slab thickness less than or equal to 50 nm should be desirable. It must be indicated that in a practical implementation, the slab thickness could be accurately controlled by using thermal oxidation after a rib etching process. Thermal oxidation is also desirable for reducing surface roughness [3].

B. Electrical Characteristics

The electrical analysis was performed on a high-index-contrast rib waveguide having $h_s = 50 \text{ nm}$ and $w_s = 200 \text{ nm}$.

1) *Static Characteristics*: Simulations reveal that both injected electron (N) and hole (P) concentrations are nearly equal and highly uniform throughout the waveguide core for forward bias voltages between 0.8 and 1.1 V (high injection conditions). We have assumed a surface recombination velocity of 10^2 cm/s at the interface between the Si waveguide and the surrounding SiO_2 , which corresponds to Si surfaces passivated with thermally grown SiO_2 [16]. A carrier concentration of approximately $N = P = 3 \times 10^{17} \text{ cm}^{-3}$ ($\Delta n = -10^{-3}$) is predicted for a forward bias of 0.87 V . The drive current for

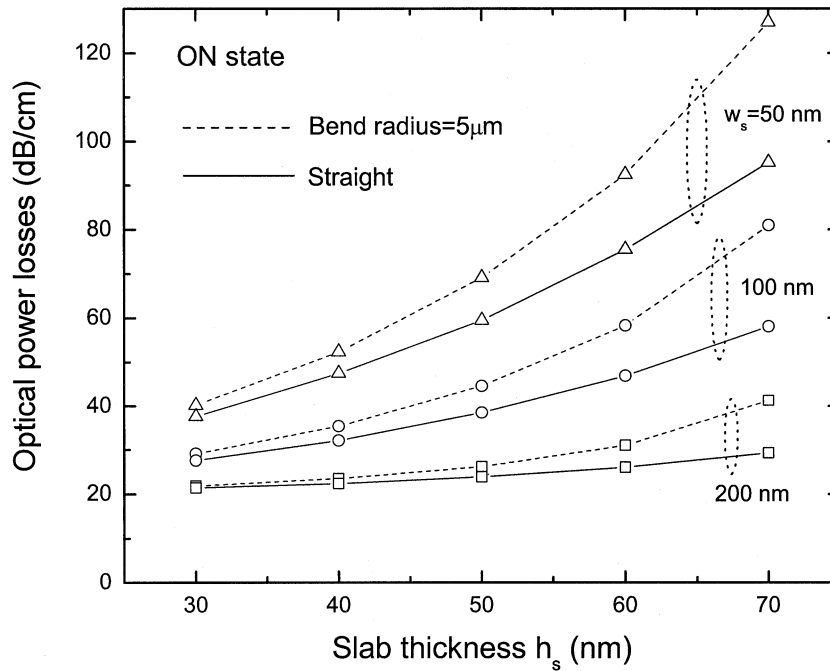


Fig. 4. Optical losses in a straight rib (solid line) and in a bent (dashed line) high-index-contrast waveguide as a function of the slab thickness (h_s) in the ON state ($\Delta n = -10^{-3}$) for w_s equal to 200 nm (square dots), 100 nm (circular dots), and 50 nm (triangular dots).

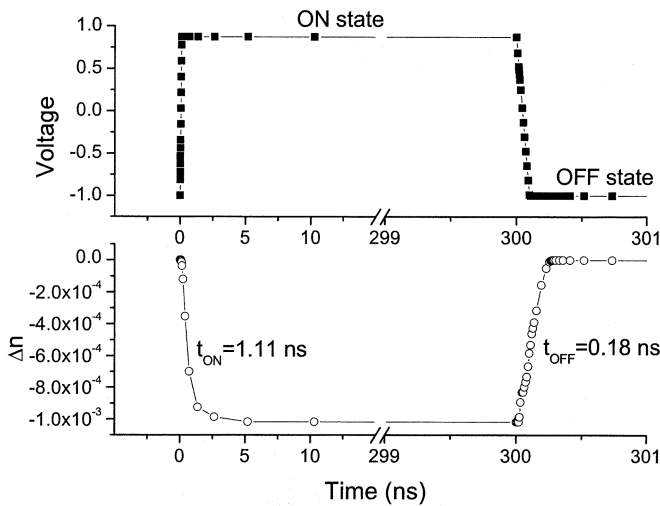


Fig. 5. Transient behavior of the refractive index change in the high-index-contrast rib waveguide for a voltage pulse with $V_{ON} = 0.87$ V and $V_{OFF} = -1$ V. In both cases, the voltage pulse is 300 ns long for both ON and OFF states with ramp and fall times of 0.1 ns.

0.87 V was calculated to be $1.76 \mu\text{A}/\mu\text{m}$, which corresponds to a dc power consumption of $1.53 \mu\text{W}/\mu\text{m}$. This low dissipated power leads to a negligible increase of the device temperature, less than 10^{-2} K.

If the Si waveguide surfaces are not passivated, both the power consumption and carrier concentration are significantly affected. Thus, for $S_p = S_n = 10^5$ cm/s (no surface passivation [16]) and a bias voltage of 0.87 V, the drive power is increased to $7.66 \mu\text{W}/\mu\text{m}$ whereas the carrier concentration is decreased to 7.3×10^{16} cm $^{-3}$.

The effect of the contact resistance of the electrodes on the total power is not significant for a forward injection current of

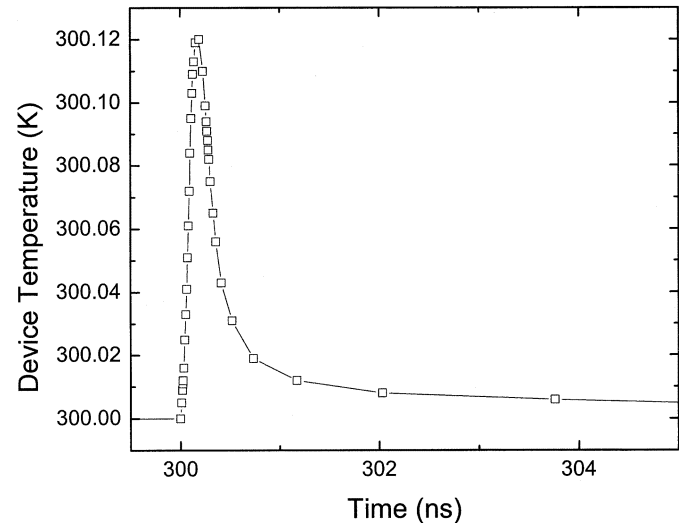


Fig. 6. Maximum device temperature transient response when the device is switched off from $V_{ON} = 0.87$ V to $V_{OFF} = -1$ V. The temperature of the thermal contacts (electrodes) is 300 K.

$1.76 \mu\text{A}/\mu\text{m}$, if proper contact metallization is achieved. For example, if Co/Si contacts are assumed on both electrodes, the corresponding contact resistance values, after a rapid thermal annealing process, on the highly doped n^+ and p^+ regions should be around $1.6 \times 10^{-7} \Omega\text{cm}^2$ and $8.9 \times 10^{-7} \Omega\text{cm}^2$, respectively [17]. This would lead to a negligible increase of 3.2×10^{-10} W per μm -length in dc power consumption for $w_d = 1 \mu\text{m}$.

2) *Transient Characteristics:* Fig. 5 shows the simulated excitation voltage pulse and the calculated refractive index variation in the intrinsic Si core due to free-carrier dispersion effect versus time. For the voltage excitation, the duration of both OFF and ON states is 300 ns, whereas both the rise time and fall time

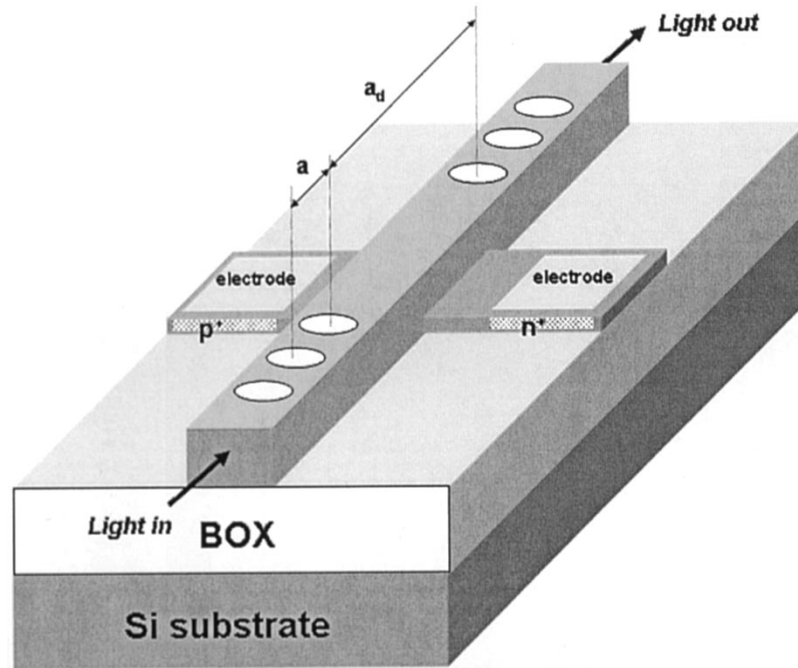


Fig. 7. Straight waveguide modulator based on a microcavity (1-D photonic crystal resonator). a is the period of the photonic crystal and a_d is the “defect” length. The complex refractive index of the resonant region is changed by free carrier plasma dispersion effect produced by a lateral integrated p-i-n diode.

for the voltage bias step are 0.1 ns. For the refractive index variation, we define the turn-on time (t_{ON}) as the time required for Δn to change from 10% to 90% of its maximum absolute value ($|\Delta n|$). Likewise, the turn-off time (t_{OFF}) is defined as the time needed for the refractive index change to vary from 90% to 10% of its maximum absolute value. The values of t_{ON} and t_{OFF} for a voltage pulse with $V_{ON} = 0.87$ V ($\Delta n = -10^{-3}$) and $V_{OFF} = -1$ V are 1.11 and 0.18 ns, respectively. As pointed out in our previous work [7], carrier diffusion and carrier depletion due to the reverse electric field are the limiting mechanisms for carrier injection (t_{ON}) and carrier removal (t_{OFF}), respectively. Due to the small volume of the guiding intrinsic region, the calculated switching time ($t_{ON} + t_{OFF} = 1.29$ ns) is one order of magnitude smaller than those reported for larger rib structures [7], [18].

An increase in the device temperature for a p-i-n/rib structure occurs during the transition from the ON state to the OFF state, due to a significant increase of the transient reverse current [7]. The maximum device temperature in the studied device is shown in Fig. 6 for $V_{OFF} = -1$ V. The maximum increase is 0.12 K and drops by one order of magnitude in 1.17 ns. This indicates an efficient heat removal through the thermal contacts and a negligible thermo-optic effect.

V. EXAMPLE: ONE-DIMENSIONAL MICROCAVITY MODULATOR

The transmission near the resonance wavelength of an optical cavity is highly sensitive to small index changes, making it ideal for intensity modulation in a short length [7]. Thus, an immediate application of the studied configuration is a straight waveguide intensity modulator based on a microcavity [6] (see Fig. 7). The device shown in Fig. 7 consists of a high-index-contrast rib SOI waveguide in which air (or SiO_2 -filled) holes

have been defined in order to provide a high-index-contrast periodic structure [one-dimensional (1-D) photonic crystal]. Details about its principle of operation and typical dimensions can be found in [6]. The studied lateral p-i-n diode configuration is used to change the refractive index in the cavity region by $\Delta n = -10^{-3}$. w_s and h_s are equal to 200 and 50 nm, respectively.

An estimation of the performance of the device shown in Fig. 7 can be made assuming that the microcavity is equivalent to a Fabry–Perot (F–P) cavity defined by distributed Bragg reflectors of reflectivity R , diffraction losses D , cavity length a_d , and internal losses A_c . We calculated the spectral characteristics of the resonator by using

$$T(\lambda) = T_{lm}(1-D) = \left(\frac{A_c(1-R)^2}{(1-A_cR)^2 + 4A_cR \sin^2\left(\frac{2\pi n_{eff} a_d}{\lambda}\right)} \right) \cdot (1-D) \quad (3)$$

where T is the transmittivity, λ is the wavelength, T_{lm} is the spectral transmittivity of the lossless-mirrors F–P cavity [19] and n_{eff} is the effective refractive index of the waveguide. We considered the following values: $R = 97\%$, $D = 17\%$ (both values were estimated from [6]), $a_d = 9.14 \mu\text{m}$ [$\approx 15(\lambda_r/2n_{eff})$], with $\lambda_r = 1.55 \mu\text{m}$ and A_c equals 4.08 and 23.86 dB/cm for the OFF state ($\Delta n = 0$) and ON state ($\Delta n = -10^{-3}$), respectively (Section IV-A2). The modulation depth, defined as $(P_{OFF} - P_{ON})/P_{OFF}$ (where P_{OFF} and P_{ON} are the transmitted power in the OFF and ON states, respectively), is predicted to be 80% at $\lambda = 1.55 \mu\text{m}$. The dc electrical power needed to achieve this high modulation depth would be around 13.98 μW (Section IV-B1), with a switching time of ~ 1.3 ns (Section IV-B2).

TABLE II
SILICON ELECTROOPTIC MODULATORS RECENTLY PROPOSED IN THE LITERATURE (FCAM = FREE CARRIER ABSORPTION MODULATOR; F-P = FABRY-PÉROT; M = AMPLITUDE MODULATION DEPTH; t_s = switching time)

Year	Author	Electrical structure	Optical structure	M (%)	Power (mW)	t_s (ns)	Length (μm)
1997	Cutolo et al. [18]	p-i-n	Bragg reflector	50	4	24.7	3200
1997	Cutolo et al. [15]	BMFET	FCAM	20	126	6	1000
2000	Irace et al. [21]	BMFET	Y-junction	92	~350	16	5000
2001	Coppola et al. [23]	p-i-n	Bragg reflector	94	0.3	5	3200
2003	Barrios et al. [7]	p-i-n	F-P	80	0.025	16	20
2003	Our device	p-i-n	F-P	80	0.014	1.3	10

For the sake of comparison, Table II shows a list of proposed silicon electrooptic modulators recently reported in the literature. It is seen that the device analyzed in this paper introduces improvements in terms of dc power consumption, switching time, and length as compared to previous works. In addition, unlike most of the other listed devices, our device can be implemented in highly dense photonic systems due to its high lateral index contrast.

VI. CONCLUSION

An electrooptic SOI high-index-contrast rib waveguide has been proposed and analyzed. The real refractive index and absorption coefficient of the core Si waveguide is changed by using the free-carrier dispersion effect produced by a lateral p-i-n diode. The simulations indicate that, for a typical single-mode high-index-contrast rib waveguide, the slab thickness and the distance of the highly doped regions to the rib should be chosen ≤ 50 nm and ≥ 200 nm, respectively, in order to minimize the losses due to the n^+ and p^+ regions. The electrical analysis predicts a dc power consumption of $1.53 \mu\text{W}/\mu\text{m}$ for inducing a refractive index change of -10^{-3} , which leads to a negligible thermo-optic effect. The switching time is calculated to be 1.29 ns for a voltage pulse between -1 and 0.87 V. These characteristics make the studied configuration very promising for implementing Si-based submicrometer-size active devices and should represent an important step in the development of high dense Si photonic circuits.

REFERENCES

- [1] L. C. Kimerling, "Photons to the rescue: microelectronics becomes microphotonics," *Electrochem. Soc. Interface*, p. 28, Summer 2000.
- [2] K. K. Lee, "Transmission and routing of optical signals in on-chip waveguides for silicon microphotonics," Ph.D dissertation, Massachusetts Inst. of Technology, Cambridge, 2001.
- [3] K. K. Lee, D. R. Lim, and L. C. Kimerling, "Fabrication of ultralow-loss Si/SiO₂ waveguides by roughness reduction," *Opt. Lett.*, vol. 26, no. 23, p. 1888, 2001.
- [4] V. A. Almeida, R. Panepucci, and M. Lipson, "Nanotaper for compact mode conversion," *Opt. Lett.*, vol. 28, no. 15, pp. 1302–1304, 2003.
- [5] B. E. Little, J. S. Foresi, G. Steinmeyer, E. R. Thoen, S. T. Chu, H. A. Haus, E. P. Ippen, L. C. Kimerling, and W. Greene, "Ultra-compact Si – SiO₂ microring resonator optical channel dropping filters," *IEEE Photon. Technol. Lett.*, vol. 10, no. 4, pp. 549–551, 1998.
- [6] J. S. Foresi, P. R. Villeneuve, J. Ferrera, E. R. Thoen, G. Steinmeyer, S. Fan, J. D. Joannopoulos, L. C. Kimerling, H. I. Smith, and E. P. Ippen, "Photonic-bandgap microcavities in optical waveguides," *Nature*, vol. 390, p. 143, 1997.

- [7] C. Angulo Barrios, V. R. Almeida, and M. Lipson, "Low-power-consumption short-length and high-modulation-depth silicon electro-optic modulator," *J. Lightwave Technol.*, vol. 21, no. 4, pp. 1089–1098, 2003.
- [8] C. Z. Zhao, A. H. Chen, E. K. Liu, and G. Z. Li, "Silicon-on-insulator asymmetric optical switch based on total internal reflection," *IEEE Photon. Technol. Lett.*, vol. 9, no. 8, p. 1113, 1997.
- [9] G. Cocorullo and I. Rendina, "Thermo-optical modulator at 1.5 μm in silicon etalon," *Electron. Lett.*, vol. 28, no. 1, p. 83, 1992.
- [10] C. Cocorullo, M. Iodice, I. Rendina, and P. M. Sarro, "Silicon thermo-optical micro-modulator with 700 kHz -3 dB bandwidth," *IEEE Photon. Technol. Lett.*, vol. 7, pp. 363–365, 1995.
- [11] R. A. Soref and B. R. Bennett, "Electrooptical effects in silicon," *IEEE J. Quantum Electron.*, vol. QE-23, no. 1, p. 123, 1987.
- [12] R. A. Soref and B. R. Bennett, "Kramers-Kronig analysis of E-O switching in silicon," *SPIE Integr. Opt. Circuit Eng.*, vol. 704, 1986.
- [13] P. D. Hewitt and G. T. Reed, "Improved modulation performance of a silicon p-i-n device by trench isolation," *J. Lightwave Technol.*, vol. 19, no. 3, p. 387, 2001.
- [14] —, "Improving the response of optical phase modulators in SOI by computer simulation," *J. Lightwave Technol.*, vol. 18, no. 3, p. 443, 2000.
- [15] A. Cutolo, M. Iodice, P. Spirito, and L. Zeni, "Silicon electro-optic modulator based on a three terminal device integrated in a low-loss single-mode SOI waveguide," *J. Lightwave Technol.*, vol. 15, no. 3, p. 505, 1997.
- [16] D. R. Lim, "Device integration for silicon microphotonic platforms," Ph.D dissertation, Massachusetts Inst. of Technology, Cambridge, 2000.
- [17] O. Nakatsuka, T. Ashizawa, H. Iwano, S. Zaima, and Y. Yasuda, "Contact resistivities and electrical characteristics of Co/Si contact by rapid thermal annealing," in *Proc. Adv. Metallization Conf. (AMC 1998)*, vol. 784, Warrendale, PA, 1999, pp. 605–610.
- [18] A. Cutolo, M. Iodice, A. Irace, P. Spirito, and L. Zeni, "An electrically controlled Bragg reflector integrated in a rib silicon on insulator waveguide," *Appl. Phys. Lett.*, vol. 71, no. 2, p. 199, 1997.
- [19] J. T. Verdeyen, *Laser Electronics*. Englewood Cliffs, NJ: Prentice-Hall, 1989, p. 137.
- [20] A. Irace, G. Coppola, G. Breglio, and A. Cutolo, "Fast silicon-on-silicon optoelectronic router based on a BMFET device," *IEEE J. Select. Topics Quantum Electron.*, vol. 6, no. 1, pp. 14–18, 2000.
- [21] G. Coppola, A. Irace, M. Iodice, and A. Cutolo, "Simulation and analysis of a high-efficiency silicon optoelectronic modulator based on a Bragg mirror," *Opt. Eng.*, vol. 40, no. 6, pp. 1076–1081, 2001.

C. Angulo Barrios is a native of Spain. He received the Telecommunications Engineer degree from the Universidad Politécnica de Madrid (UPM), Madrid, Spain, in 1998, and the Ph.D. degree from the Royal Institute of Technology (KTH), Stockholm, Sweden, in 2002. His doctoral research focused on the use of III-V semi-insulating materials for buried-heterostructure semiconductor lasers.

In May 2002, he joined the Nanophotonics group at the School of Electrical and Computer Engineering, Cornell University, Ithaca, NY, as a Postdoctoral Fellow. His research includes design, fabrication, and characterization of Si-based photonic integrated devices.

V. R. Almeida (S'03) is a native of Brazil. He received the B.S. (*magna cum laude*) and M.S. degrees, both in electrical engineering, from Instituto Tecnológico de Aeronáutica (ITA), São José dos Campos, Brazil, in 1997 and 1998, respectively. Since 2000, he has been working toward the Ph.D. degree in electrical engineering from Cornell University, Ithaca, NY.

From 1998 until 2000, he conducted research on optical fiber sensors at Instituto de Estudos Avancados (IEAv-CTA), São José dos Campos, Brazil. His research interest areas are nanophotonic devices, optical fiber sensors and photonic crystals.

Mr. Almeida is a Student Member of the Optical Society of America (OSA).

R. Panepucci received the Ph.D. degree in electrical engineering from University of Illinois at Urbana-Champaign (UIUC) with research emphasis in optical properties of III–V nanofabricated structures.

After a postdoctoral position at the University of Campinas, he joined the Cornell Nanofabrication Facility (CNF), Cornell University, Ithaca, NY, as a Senior Research Staff Member, where he managed the high-resolution ebeam system and developed nanofabrication techniques. He later spent two years in a photonic startup company as microelectromechanical (MEMS) team leader. He has also extensive teaching experience both as a Teaching Assistant at University of São Paulo (USP)-Brazil, Caltech, and UNICAMP-Brazil, and as a Professor at the University of Mogi das Cruzes, Brazil. He is now a Senior Research Associate with the Nanophotonics group at the School of Electrical and Computer Engineering, Cornell University, Ithaca, NY.

M. Lipson (M'03) received the Ph.D. degree on semiconductor microcavities from The Technion—Israel Institute of Technology, Haifa, Israel, in 1999.

She was a Postdoctoral Associate in the Material Science Department at the Massachusetts Institute of Technology (MIT), Cambridge. Her research at MIT was concerned with the physics and applications of Si-based photonic structures for on-chip applications. In July 2001, Lipson joined the School of Electrical and Computer Engineering at Cornell University, Ithaca, NY, as an Assistant Professor, where she is studying nanophotonic structures.

She is a Member of the Optical Society of America (OSA).